International Journal of Robotics and Automation, Vol. 40, No. 10, 2025
An Open Access Paper

QUASI-CAVITATION PREDICTION OF UNDERWATER THRUSTERS-BASED ON BAYESIAN ESTIMATION AND GAUSSIAN PROCESS

Li Zhandong,* Ma Shuang,** Han Qi,* Li Jingkui,* and Wang Chao***

Abstract

In order to realise thrust prediction under quasi-cavitation when the underwater thrusters working near water surface, a novel thrust prediction approach based on Bayesian estimation and Gaussian process is proposed. The Bayesian estimation based thrust model (BETM) is established to obtain the relationship between thrust, rotation speed and input current. Then, a quasi-cavitation prediction model based on Gaussian process (QCTM-GP) is established which considering thrust loss caused by quasi-cavitation, the BETM and QCTMGP are used to realise quasi-cavitation thrust prediction. The accuracy of BETM and the effectiveness of QCTM-GP is validated via experiments.

Key Words

Underwater thruster, quasi-cavitation, Bayesian estimation, Gaussian process.

1. Introduction

Most of underwater vehicles (UVs) utilise propeller-type underwater thrusters as their unique power source [1]–[3] Hence, thrust prediction of underwater thrusters with accuracy is an important factor to improve the performance of UVs. However, quasi-cavitation will frequently occur when the UV work near the water which greatly reducing the efficiency of the thruster and causing thrust loss and noise as shown in Fig. 1.

* College of Civil Aviation, Shenyang Aerospace University, Shenyang 110136, China; e-mail: lizhandong365@163.com; 1245360854@qq.com; lijingkui@sau.edu.cn
** College of Electronic and Information Engineering, Shenyang Aerospace University, Shenyang 110136, China; e-mail: 835597410@qq.com
*** School of Mechanical Engineering, Dongguan University of Technology, Dongguan 523808, China; e-mail: wangchao@dgut.edu.cn
Corresponding author: Ma Shuang

(DOI: 10.2316/J.2025.206-1040)

Up to now, several approaches are proposed to predict the thrust of underwater thrusters. The analysis of thrust is divided into numerical simulation [4]–[6] and model parameter identification [7], [8]. For numerical simulation, finite element analysis is utilised to simulate the fluid structure coupling of the propeller and some characteristics related to thrust can be obtained. The model parameter identification gets the data directly though tests to identify the model parameters.

Wu *et al.* proposed a practical approach to simulate hydrodynamic performance of ducted propeller attached in an UV under the influence of flow field of the vehicle. Computational fluid dynamics (CFD) technique based on the finite volume method and multi-sliding mesh technique are applied to solve the Navier–Stokes equations when the vehicle in a yawing motion [9]. Wang *et al.* [10] examined the characteristics of the relationship between the evolution of propeller trailing vortex wake and skew angle numerically based on four different five-blade David Taylor model basin (DTMB) model propellers with different skew angles, the simulated results shown that the contraction of propeller trailing vortex wake can be restrained by increasing skew angle and loading conditions.

In practice, the thrust model based on prediction method of underwater thrusters is a complex nonlinear function related to the rotation speed of propeller [11], [12]. For the convenience of calculation, the steady-state thrust model based on prediction method is simplified to the quadratic relationship between thrust and rotation speed in most cases which uses thrust coefficients to fit different types of propellers [13]–[15]. Tran *et al.* [16] presented the open water propeller characteristics and four-quadrant propeller models as applied to a torpedo-shaped UV. A series of experiments with a Gavia autonomous underwater vehicle propeller were conducted in the towing tank using a rotor testing apparatus. Paolucci *et al.* [17] proposed permanent magnet synchronous motors for underwater propulsion and the design and implementation of a complete solution for underwater propulsion were presented as well as a novel rotor polarity identification technique exploiting a high-frequency injection control.

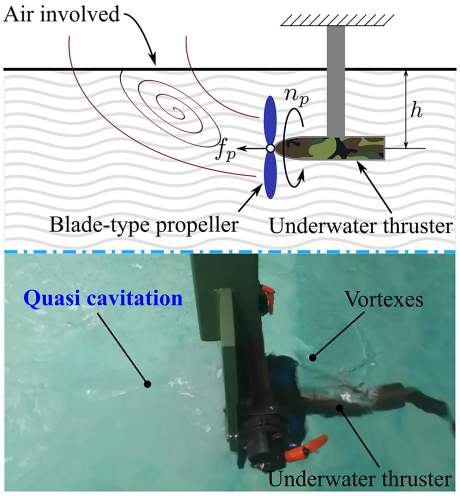

Figure 1. Schematic of quasi-cavitation.

Nevertheless, the quasi-cavitation is not considered in current researches. when quasi-cavitation occurs, it will cause thrust loss and noise. In this paper, a novel quasi-cavitation prediction model based on Bayesian estimation and Gaussian process is proposed to complete thrust prediction under quasi-cavitation. First, the Bayesian estimation based thrust model (BETM) is established to accurately predict thrust without quasi-cavitation. Then, the quasi-cavitation prediction model based on Gaussian process (QCTM-GP) is represented which considering thrust loss caused by quasi-cavitation. Finally, the accuracy of BETM and the effectiveness of QCTM-GP is validated via experiments. The proposed quasi-cavitation model based on prediction method holds a great potential on the accurate control of UVs.

2. Quasi-Cavitation Thrust Model-Based on Prediction Method

In this section, a novel quasi-cavitation thrust model based on prediction method is proposed to perform a prediction under quasi-cavitation which utilises the information of rotation speed, input current and the distance between a propeller and the water surface. The proposed quasi-cavitation thrust model based on prediction method is composed of BETM and QCTM-GP as shown in (1)

$$\widetilde{f} = \underbrace{b(n_p, I)}_{\text{BETM}} + \underbrace{g(n_p, I, h)}_{QCTM-GP} \tag{1}$$

where $\widetilde{f}$ is the output of model based on prediction method, n_p is the rotation speed of propeller, I is the input current of driver, and h is the distance between the propeller and water surface.

BETM uses Bayesian estimation method to fuse the rotation speed with an input current to obtain accurate thrust prediction without quasi-cavitation. Furthermore, QCTM-GP utilises Gaussian process to prediction thrust loss of BETM under quasi-cavitation. The structure of quasi-cavitation model based on prediction method is shown in Fig. 2.

2.1 Modelling of Underwater Thrusters

The relationship between the thrust and the rotation speed of a propeller is shown as (2) [13]

$$f_p = \rho D^4 K_f(J_0)\,|n_p|\,n_p \tag{2}$$

where f_p is the thrust of underwater thruster, ρ is the density of water, D is the diameter of propeller, J_0 is the advance number, and K_f is the thrust coefficient.

The relationship between torque and rotation speed of propeller can be expressed as (3) [13]

$$Q_p = \rho D^5 K_Q(J_0)\,|n_p|\,n_p \tag{3}$$

where Q_p is the torque of underwater thruster and K_Q is the torque coefficient.

K_f and K_Q are functions of J_0. Typically, the movement speed of the UV is slow, namely, $J_0 \approx 0$. Moreover, due to the symmetrical design of the propeller, K_f and K_Q are approximately constant, as shown in (4)

$$K_f \approx \alpha \tag{4a}$$
$$K_Q \approx \beta \tag{4b}$$

where α and β are constants.

Hence, the relationship of f_p and Q_p can be expressed as

$$f_p = \frac{\alpha}{\mathrm{D}\beta} Q_p \tag{5}$$

The underwater thruster consists of propeller, gear reducer and BLDC as shown in Fig. 3. The relationship between the rotation speed and torque of the BLDC can be expressed as (6)

$$n_e = \lambda n_p \tag{6a}$$
$$Q_p = \eta_g \lambda Q_e \tag{6b}$$

where λ is reduction ratio of the gear reducer (here is 5:1), $n_e$is the rotation speed of the BLDC, $Q_e$is the torque of the BLDC, and $\eta_g$is the efficiency of the gear reducer, usually 0.85.

The voltage balance equation of BLDC can be expressed as

$$\begin{bmatrix} u_a \\ u_b \\ u_c \end{bmatrix} = \begin{bmatrix} r & 0 & 0 \\ 0 & r & 0 \\ 0 & 0 & r \end{bmatrix} \begin{bmatrix} i_a \\ i_b \\ i_c \end{bmatrix} + \begin{bmatrix} e_a \\ e_b \\ e_c \end{bmatrix} + \begin{bmatrix} L-M & 0 & 0 \\ 0 & L-M & 0 \\ 0 & 0 & L-M \end{bmatrix} p \begin{bmatrix} i_a \\ i_b \\ i_c \end{bmatrix} \tag{7}$$

where u_* is the phase voltage, i_* is the phase current, e_* is the back electromotive force (BEMF), r is the armature resistance, L is the armature inductance, M is the mutual inductance and p is differential operator, $p = d/dt$.

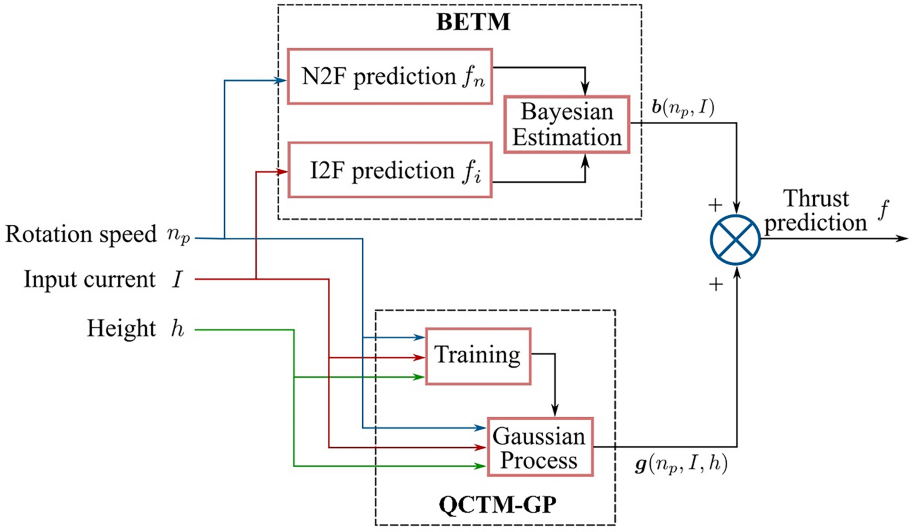

Figure 2. The structure of quasi-cavitation thrust model based on prediction method.

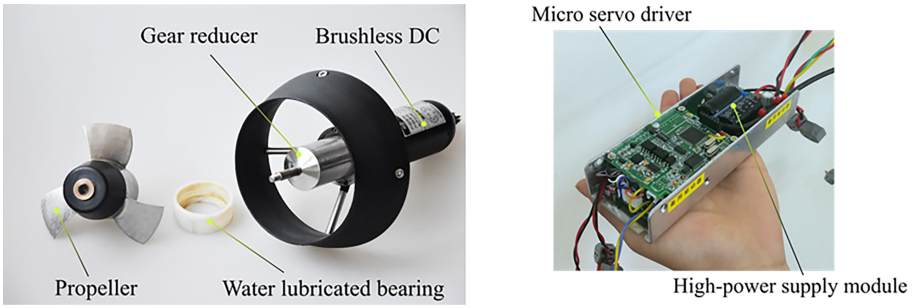

Figure 3. The underwater thruster and driver: (a) The structure of thruster and (b) The micro servo driver.

The electromagnetic torque of the BLDC satisfies the relationship shown as (8)

$$e_* = 2\pi K_e n_e \tag{8a}$$
$$T_e = K_e i_* \tag{8b}$$

where $T_e$is the electromagnetic torque of the BLDC and $K_e$is the torque constant.

Consequently, the dynamic model of the BLDC under speed control can be expressed as (9)

$$L\frac{di_*}{\mathrm{dt}} = -ri_* - 2\pi K_e n_e + u_* \tag{9a}$$
$$2\pi J_e \frac{dn_e}{\mathrm{dt}} = K_e i_* - Q_L - Bn_e \approx K_e i_* - Q_e \tag{9b}$$

where $J_e$is the inertia of the BLDC, B is the damping coefficient, and $Q_L$is the loading moment, Q_L= Q_e.

The electromagnetic power of the BLDC $P_e$is shown as (10)

$$Pe \approx \sqrt{3} e_* i_* = T_e n_e \tag{10}$$

Furthermore, the relationship between input power and electromagnetic power of the BLDC can be expressed as (11)

$$P_e = P\cos\varphi = UI\cos\varphi \tag{11}$$

where P is the input power of BLDC, cosφ is the power factor (usually 0.85 $\sim$ 0.95), U is the input voltage of driver, and I is the input current of driver.

At the steady state, Q_e= T_e= $K_e i_*$. Hence,

$$I = \frac{T_e n_e}{U\cos\varphi} = \frac{\rho D^5 K_Q |n_p|^3}{\eta_g U\cos\varphi} = C_n |n_p|^3 \tag{12}$$

where C_n= $\rho D^5 K_Q/(\eta_g U$ cos$\varphi)$ is constant at the steady state which indicates that the input current is proportional to the cube of the rotation speed. Therefore, the relationship between an input current, the rotation speed, and the thrust are shown in (13)

$$I = \frac{DK_Q}{K_T \eta_g U\cos\varphi} f_p n_p = C_T f_p n_p \tag{13}$$

where C_T= $DK_Q/(K_f \eta_g U$ cos$\varphi)$ is constant at the steady state.

Thus, the relationship between $f_p$and I can be expressed as

$$f_p = C_i I^{\frac{2}{3}} \tag{14}$$

where C_i is the current coefficient.

2.2 Bayesian Estimation-Based Thrust Model

From (2) to (14), the thrust can be predicted by rotation speed or input current individually. In order to perform more accurate thrust prediction, BETM is proposed which uses Bayesian estimation to fuse the rotation speed with the input current to obtain more accurate thrust prediction.

Assume that the data set of a rotation speed $F_N$and the data set of an input current $F_I$are Gaussian distribution, where $f_n$and $f_i$represent the rotation speed and the input current in a certain measurement, respectively.

To measure the deviation between $f_n$and f_i, Define confidence measures $d_{ni}$and d_{in}as

$$d_{\mathrm{ni}} = 2\int_{n}^{i} p_n(\ f|\, f_n)\mathrm{dx} \tag{15a}$$

$$d_{\mathrm{in}} = 2\int_{i}^{n} p_i(\ f|\, f_i)\mathrm{dx} \tag{15b}$$

where $p_n(f|f_n)$ and $p_i(f|f_i)$ are probability density function of $f_n$and $f_i$which satisfy the following conditions

$$P_*(\ f|\, f_*) = \frac{1}{\sqrt{2\pi}\sigma_*} e^{-\frac{1}{2}\left(\frac{f-f_*}{\sigma_*}\right)^2} \tag{16}$$

where σ_* is mean square error of measurement data, $\sigma_* = E\{[x - E(x)]^2\}$.

$d_{ni}$and d_{in} represent the degree of fusion between the two data sets. The smaller the value of d, the closer the thrust obtained by either method. Thus, the confidence matrix $\boldsymbol{D}$ can be expressed as

$$D = \begin{bmatrix} d_{\mathrm{nn}} & d_{\mathrm{ni}} \\ d_{\mathrm{in}} & d_{\mathrm{ii}} \end{bmatrix} \tag{17}$$

Thrust model can be obtained by rotation speed and input current, respectively. To determine whether the thrust prediction results obtained by the two methods are compatible, the fusion coefficient γ is introduced to divided the confidence measure d

$$\delta = \begin{cases} 1 & (d \le \gamma) \\ 0 & (d > \gamma) \end{cases} \tag{18}$$

where γ is the fusion coefficient. When $\gamma = 0$, it means that the two thrust prediction results are of poor compatibility and one of them must be eliminated. If $\gamma = 1$, the two thrust prediction results are well compatible, and the two results can be compatible. Therefore, the Bayesian estimation value of the thrust f is:

$$d(f_n, f_i) = \mathbb{R}(\ f|\, f_n, f_i) = \int \mathrm{fp}(\ f|\, f_n, f_i)\mathrm{df} \tag{19}$$

where the conditional probability density function $p(f|f_n, f_i)$ is unknown, but it can be expressed by (20)

$$p(\ f|\, f_n, f_i) = \frac{p(f, f_n, f_i)}{p(f_n, f_i)} \tag{20}$$

where $f \sim \mathcal{N}(u_0, \sigma_0^2)$, $f_n \sim \mathcal{N}(u, \sigma_n^2)$, $f_i \sim \mathcal{N}(u, \sigma_i^2)$. According to the Bayes Formula, let $\beta = 1/p(f_n, f_i)$,

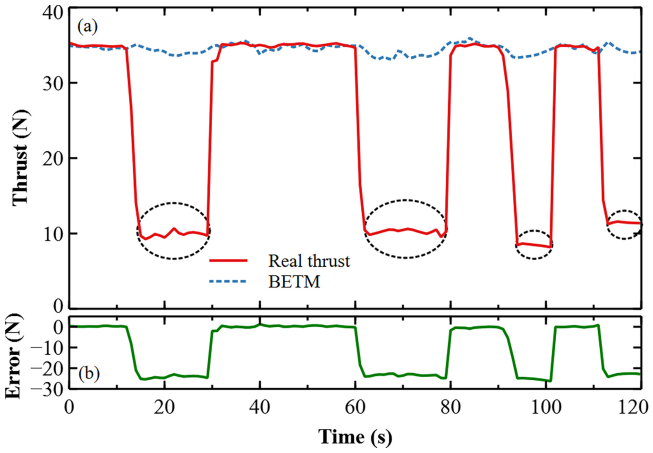

Figure 4. The prediction error of BETM: (a) The performance of BETM under quasi-cavitation and (b) The prediction error of BETM.

$p(f|f_n, f_i)$ can be written as

$$p(\ f|\, f_n, f_i) = \beta \frac{1}{\sqrt{2\pi}\sigma_0} e^{-\frac{1}{2}\frac{(f-u_0)}{\sigma_0^2}} \prod_{k\in\{f_n,f_i\}} \frac{1}{\sqrt{2\pi}\sigma_k} e^{-\frac{1}{2}\sum_{k\in\{f_n,f_i\}}\frac{(x_k-u)^2}{\sigma_k^2}} \tag{21}$$

By (21), $p\ (f|f_n, f_i)$ is Gaussian distribution, *i.e.*, $f \sim N(u_n, \sigma_n)$. Hence, BETM can be expressed as the following form

$$f = b(n_p, I) = \frac{\sum_{k\in\{f_n,f_i\}}\frac{x_k}{\sigma_k^2} + \frac{u_0}{\sigma_0^2}}{\sum_{k\in\{f_n,f_i\}}\frac{1}{\sigma_k^2} + \frac{1}{\sigma_0^2}} \tag{22}$$

2.3 Quasi-Cavitation Prediction Model-Based on Gaussian Process

BETM can perform accurate thrust prediction without quasi-cavitation. However, BETM can cause large prediction error under quasi-cavitation effect. Therefore, a QCTM-GP is presented to learn the prediction error of BETM *via* Gaussian process and achieve accurate thrust prediction under quasi-cavitation.

Let $\widehat{f}$ be the actual thrust of the underwater thruster and f be the prediction thrust of BETM. Therefore, the prediction error of BETM f_{error} can be written as

$$f_{\mathrm{error}} = \widehat{f} - f \tag{23}$$

Thrust loss increases due to the decrease of the efficiency of the propeller under quasi-cavitation, for example, when the rotation speed $n_p = 1500\ r/\mathrm{min}$, the distance between a propeller and the water surface $h = 50$ cm, the prediction error of BETM increases correspondingly as shown in Fig. 4.

In order to realise accurate thrust prediction under quasi-cavitation, the prediction error of BETM f_{error} is selected as the output of GP based model as (24)

$$g(x) = f_{\mathrm{error}} \sim \mathrm{GP}(m, \kappa) \tag{24}$$

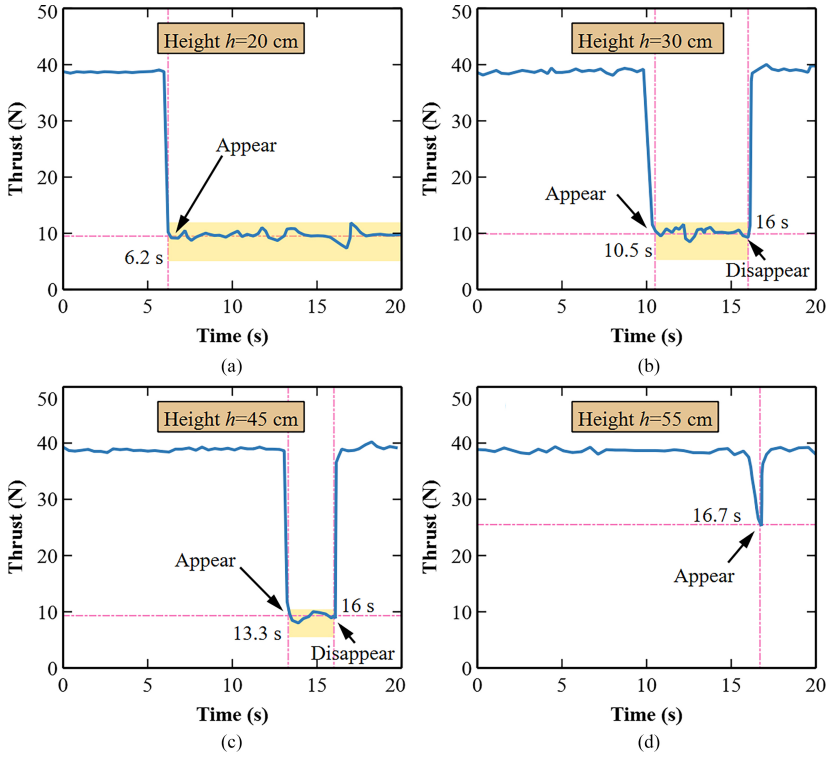

Figure 5. The impact analysis of the distance between propeller and surface.

where $g(x)$ is the function of the prediction error, m is the mean function of GP, κ is the covariance function of GP.

In the feature selection of GP, the rotation speed of the propeller $n_p$and the input current I are selected to be the input feature, namely $(n_p,\ I) \rightarrow f_{error}$. Meanwhile, the probability of quasi-cavitation is also related to the distance between the propeller and water surface as shown in Fig. 5.

As shown in Fig. 5, the underwater thruster remains the rotation speed at about 1404 r/min and adjusts the distance between the propeller and water surface h. When h is 20 cm [Fig. 5(a)], quasi-cavitation appears at 6.2 s, the thrust decreases from 38 N to 9.8 N. When h is 30 cm [Fig. 5(b)], quasi-cavitation appears at 10.5 s and disappears at 16 s. When h is 45 cm [Fig. 5(c)], quasi-cavitation appears at 13.3 s and disappears after 2.7 s. Finally, when h is 55 cm [Fig. 5(d)], quasi-cavitation appears at 16.7 s and disappears soon.

Therefore, h is selected as the input feature of GP. Let $D = \{(x_i, y_i)|i = 1,...,n\}$ be the training set, where x_i=(n_{pi}, I_i, h_i) and $y_i = f_{error}$.

QCTM-GP can be expressed as (25)

$$\Delta f = GP(m, \kappa) = g(n_p, I, h) \tag{25}$$

The training set can be expressed as

$$D = \{\ (x_i, y_i)|\ i = 1, 2, ..., n\} \tag{26}$$

where $x_i \in \mathrm{R}^d$ is a set of d dimension input vectors in the $d \times n$ dimension input matrix x. And $y_i$represents a set of observations in $1 \times n$ dimension observation matrix of thrust.

Consequently, the training set can be represented as $\boldsymbol{D}$ = $(x,\ y)$. Furthermore, each sample is weighted accordingly with ω_i. Let ω be the n-th diagonal matrix

$$\omega = \begin{bmatrix} \omega_1 & 0 & \cdots & 0 \\ 0 & \omega_2 & \cdots & 0 \\ \vdots & \vdots & \ddots & \vdots \\ 0 & 0 & \cdots & \omega_n \end{bmatrix} \tag{27}$$

Assume that the QCTM-GP has the following form

$$g(x_i) = \phi(x_i)^T \alpha_i \tag{28}$$

where $\varphi(\cdot)$ is nonlinear mapping function, $\alpha_i$is parameter vector which satisfies the Gaussian prior distribution with mean $\mathbf{0}$ and covariance matrix Σ_p, namely

$$\alpha \sim N\left(0, \sum_p\right) \tag{29}$$

Assume that ε is the noise between the observation $y_i$and the output of QCTM-GP $g(x_i)$. Then the weighted estimation model can be expressed as

$$\omega_i y_i = \omega_i g(x_i) + \varepsilon \tag{30}$$

Assume that ε follows an independent Gaussian distribution with mean 0 and variance σ_n^2 as (31)

$$\varepsilon \sim N(0, \sigma_n^2) \tag{31}$$

Considering the weighted function and noise, the Bayesian model is introduced to predict the output of GP

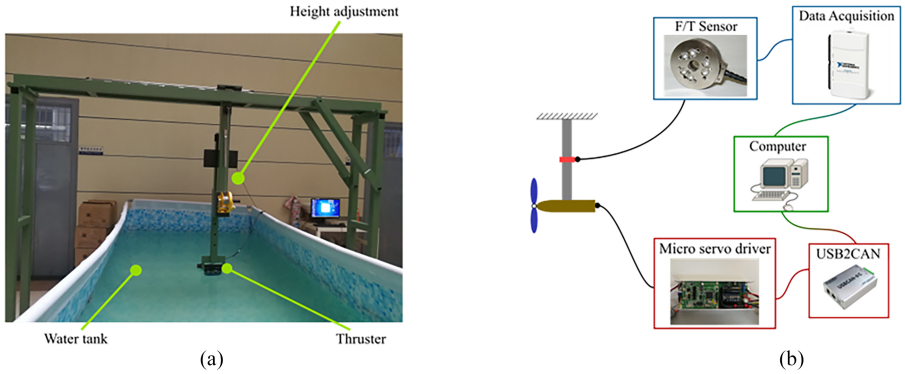

Figure 6. The experimental facility for thrust experiments: (a) The structure of experimental facility and (b) The structure of data acquisition system.

g_* which can be given by

$$p(\ g_*|\, x_*, x, y) = \int p(\ g*|\, x_*, \omega) p(\ \omega|\, x, y)$$
$$\sim N\left(\frac{1}{\sigma_n^2}\phi(x_*)^T B^{-1}\phi(x)\omega^2 y, \phi(x_*)^T B^{-1}\phi(x_*)\right) \quad (32)$$

where $B = \sigma_n^{-2}\,\phi(x)\,\omega^2\phi(x)^T + \Sigma_p^{-1}$. Let k satisfy $k(x, x^T) = \varphi(x^T)\Sigma_p\varphi(x)$. According to the characteristics of covariance matrix, $\Sigma_p$is the positive definite matrix.

Then $\left(\Sigma_p^{1/2}\right)^2 = \Sigma_p$. Define $\varphi(x) = \Sigma_p^{1/2}\phi(x)$ and it can be obtained that $k(x, x^T) = \varphi(x)\varphi(x^T)$. The covariance matrix can be defined as $k = \varphi(x)\Sigma_p\varphi(x^T)$. Then

$$\frac{1}{\sigma_n^2}\phi(x)(\omega^2 k + \sigma_n^2 I_n) = B\sum_p \phi(x) \quad (33)$$

Let (33) pre-multiplication by B^{-1} and post-multiplication by $(\omega^2 k + \sigma^2 I_n)^{-1}$

$$\frac{1}{\sigma_n^2}B^{-1}\phi(x) = \sum_p \phi(x)(\omega^2 k + \sigma_n^2 I_n\ )^{-1} \quad (34)$$

Hence, The posterior distribution mean of g_* can be rewritten as:

$$\frac{1}{\sigma_n^2}\phi(x^*)^T B^{-1}\phi(x)\omega^2 y = k(x^*, x)(\omega^2 k + \sigma_n^2 I_n)^{-1}\omega^2 y \quad (35)$$

According to Sherman – Morrison – Woodbury theorem, the posterior distribution covariance of f^* can be rewritten as

$$\phi(x^*)^T\left(\frac{1}{\sigma_n^2}\phi(x)\omega^2\phi^T(x) + \Sigma_p^{-1}\right)^{-1}\phi(x^*)$$
$$= k(x^*, x^*) - k(x^*, x)$$
$$* \left(k(x, x) + \omega^{-1}\sigma_n^2 I_n\omega^{-1}\right)^{-1} k(x, x^*) \quad (36)$$

Therefore, QCTM-GP can be expressed as

$$g^*|\, x^*, x, y \sim N(k(x^*, x)(\omega^2 k + \sigma_n^2 I_n)^{-1}\omega^2 y, k(x^*, x^*)$$
$$-k(x*, x) * (k(x, x) + \omega^{-1}\sigma_n^2 I_n\omega^{-1})^{-1}k(x, x^*)) \quad (37)$$

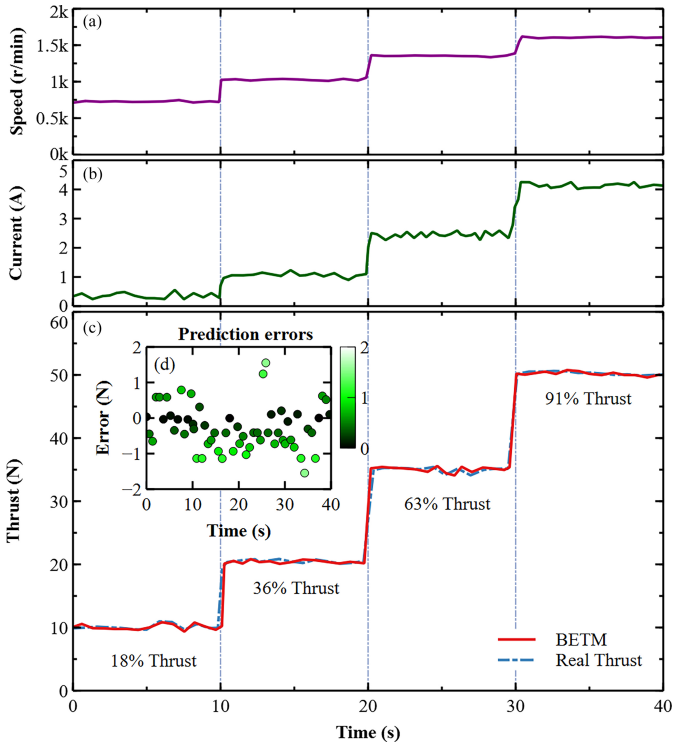

Figure 7. The experimental results of BETM: (a) The curve of rotation speed np over time, (b) The curve of input current I over time, (c) The curve of thrust f over time. The blue dash line is the real thrust and the red solid line is the thrust prediction of BETM and (d) The prediction error of BETM.

3. Experimental Verifications

Experiments are set up to validate the accuracy of BETM and the effectiveness of QCTM-GP as shown in Fig. 6. High-speed data acquisition is achieved by ATI's mini 45 F/T sensor and NI's DAQ6210 data acquisition card. BLDC is utilised for the underwater thruster with the power of 350 W, and the maximum thrust of underwater thruster is 55 N.

To validate the accuracy of BETM, several experiments have done under different thrust commands as shown in Fig. 7. The thrust predictions of 18%, 36%, 63% and

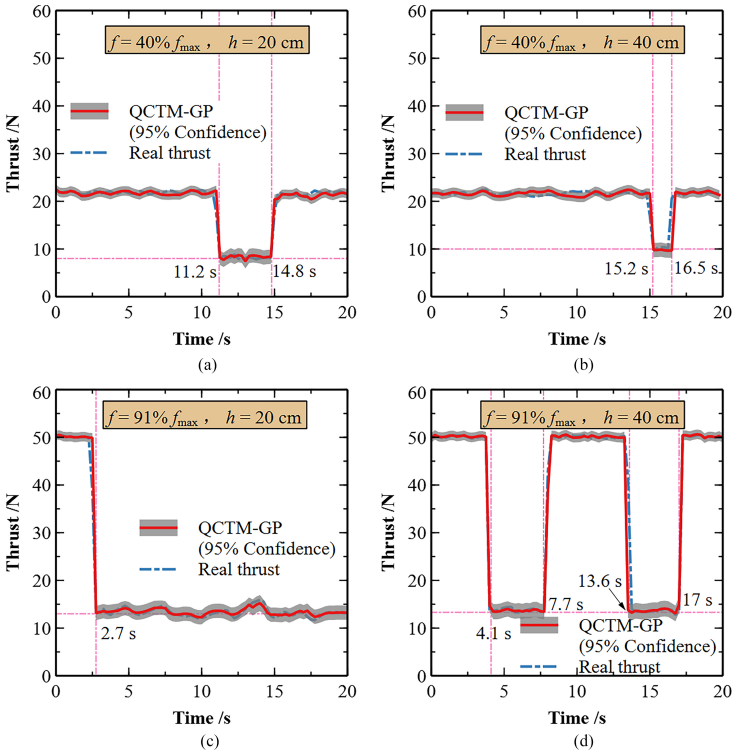

Figure 8. The experimental results of QCTM-GP. The blue dash lines are the real thrust, the red solid lines are the thrust prediction of QCTM-GP and the gray areas are the 95% confidence of QCTM-GP. The two subfigures in each row describe the performance of QCTM-GP with the same thrust command and different h under quasi-cavitation. The two subfigures in each column describe the performance of QCTM-GP with different thrust commands and the same h under quasi-cavitation.

91% thrust commands are verified in the experiments, respectively. As shown in Fig. 7(a) and (b), the fluctuation of current is greater than that of rotation speed. Therefore, the thrust prediction obtained by rotation speed in BETM has higher weight than that obtained by input current.

For example, at 18% thrust command in 0 s∼10 s, thrust is at about 10 N as shown in Fig. 7(c). But there is fluctuation of thrust at 7 s. Due to the integration of input current information, BETM accurately predicts the change of thrust within the error of 1 N. Hence, BETM can perform thrust prediction with accuracy *via* fusing the two predictions based on Bayesian estimation.

To further verify the accuracy of BETM, the error of BETM is analysed as shown in Fig. 7(d). The lighter the point's color, the larger the point's error. From the error distribution of BETM, the maximum error is less than 2 N. Moreover, 75% of the errors are within 1 N. Therefore, BETM can perform accurate thrust prediction without quasi-cavitation.

To demonstrate the effectiveness of QCTM-GP, quasi-cavitation thrust predictions via QCTM-GP are presented at different thrust commands and different h as presented in Fig. 8.

It can be seen from the subfigures of each row that the occurrence probability and duration of quasi-cavitation significantly decrease with the increasement of the distance between propeller and water surface. When the thrust command is 40% and h is 20 cm, quasi-cavitation appears at 11.2 s and disappears after 3.6 s. When h increase to 40 cm, quasi-cavitation appears at 15.2 s and disappears after 1.3 s. From the subfigures of each column, the occurrence probability and duration of quasi-cavitation significantly increase with the increase of rotation speed.

When h is 20 cm and thrust command is 40%, quasi-cavitation appears at 11.2 s, while under 91% thrust command, quasi-cavitation appears at 2.7 s. The experimental results demonstrate the correctness of feature selection in GP.

As shown in Fig. 8, thanks to the accurate prediction of BETM, thrust model based on prediction method can accurately predict the thrust without quasi-cavitation. The confidence of GP remains ± 1 N and the errors are less than 2 N. When quasi-cavitation occurs, although BETM cannot perform the thrust prediction with accuracy, the thrust loss can be compensated by QCTM-GP with the 95% confidence of ± 1.7 N and error less than 3.5 N which satisfy the accuracy requirement of UVs' control system for underwater thrusts.

4. Conclusions

In this paper, a novel thrust prediction approach is proposed to accurately obtain the thrust loss with quasi-cavitation effect. First, the underwater thruster is modelled, which can establish the relationship between the thrust and the rotation speed, an input current. Second, the BETM is applied without quasi-cavitation. Then, a QCTM-GP is established, which can consider thrust loss due to quasi-cavitation, and the thrust prediction model is obtained based on BETM and QCTM-GP. Finally, the

accuracy of BETM and the effectiveness of QCTM-GP is validated by experiments, the results show that quasi-cavitation model based on prediction method can perform a precise thrust prediction, and the error is within 3.5 *N*, which can satisfy the accuracy requirements of UVs' control system.

Acknowledgement

The author(s) disclose receipt of the following financial support for the research, authorship, and/or publication of this article. This work was support by Natural Science Foundation of Liaoning Province of China (No. 2022-BS-216) and Science Star-up Foundation for Introduced Talent of Shenyang Aerospace University (No. 18YB35), the National Natural Science Foundation of China (No. 52005104).

References

[1] Z. Huang, L. Wan, M. Sheng, J. Zou, J. Song. An underwater image enhancement method for simultaneous localisation and mapping of autonomous underwater vehicle, *2019 3rd International Conference on Robotics and Automation Sciences (ICRAS)*, IEEE, 2019, 137-142.

[2] J. Wang, S. Bai, B. Englot, Underwater localisation and 3D mapping of submerged structures with a single-beam scanning sonar, *2017 IEEE International Conf. on Robotics and Automation (ICRA)*, IEEE, 2017, 4898-4905.

[3] A. Jebelli, A. Mahabadi, H. Chaoui, Tracking and mapping system for an underwater vehicle in real position using sonar system, *International Journal of Robotics and Automation*, 37(1), 2022, 124-134.

[4] H. Seol, J.-C. Suh, S. Lee, Development of hybrid method for the prediction of underwater propeller noise, *Journal of Sound and Vibration*, *288*(1-2), 2005, 345-360.

[5] J. Kim, W.K. Chung, Accurate and practical thruster modelling for underwater vehicles, *Ocean Engineering*, 33(5-6), 2006, 566-586.

[6] O. Xie, B. Li, K. Huang, Q. Yan, Three-dimensional hydrodynamics simulation and experimental on a bio-inspired underwater hybrid propeller, *International Journal of Robotics and Automation*, 33(3), 2018, 1-9.

[7] L.L. Whitcomb, D.R. Yoerger, Development, comparison, and preliminary experimental validation of nonlinear dynamic thruster models, *IEEE Journal of Oceanic Engineering*, *24*(4), 1999, 481-494.

[8] R. Bachmayer, L.L. Whitcomb, Adaptive parameter identification of an accurate nonlinear dynamical model for marine thrusters, *Journal of Dynamic Systems, Measurement, and Control*, *125*(3), 2003, 491-494.

[9] J. Wu, C. Zhang, Z. Ye, Y. Xu, W. Feng, H. Liang, Numerical simulation on hydrodynamic behaviours of ducted propeller in yawing motion of an underwater vehicle, *International Conf. on Offshore Mechanics and Arctic Engineering. American Society of Mechanical Engineers*, 2015, 56598, V011T12A025.

[10] L.-Z. Wang, C.-Y. Guo, Y.-M. Su, T.-C. Wu, A numerical study on the correlation between the evolution of propeller trailing vortex wake and skew of propellers, *International Journal of Naval Architecture and Ocean Engineering*, *10*(2), 2018, 212-224.

[11] M. Blanke, K.-P. Lindegaard, T.I. Fossen, Dynamic model for thrust generation of marine propellers, *IFAC Proceedings Volumes*, *33*(21), 2000, 353-358.

[12] A.S.A. Doss, D. Venkatesh, M. Ovinis, Simulation and experimental studies of a mobile robot for underwater applications, *International Journal of Robotics and Automation*, 36(1), 2021, 10-17.

[13] T.I. Fossen, *Guidance and control of ocean vehicle* (New York: Wiley, 1994), 108-120.

[14] W. Gan, D. Zhu, S.X. Yang, A Speed Jumping-free Tracking Controller with Trajectory Planner for Unmanned Underwater Vehicle, *International Journal of Robotics and Automation*, *35*(5), 2020.

[15] M.L. Buhl Jr., New empirical relationship between thrust coefficient and induction factor for the turbulent windmill state. *National Renewable Energy Laboratory. (NREL)*, Golden, CO (United States), Technical Report NREL/TP-500-36834 August 2005.

[16] M. Tran, J. Binns, S. Chai, A.L. Forrest, H. Nguyen, A practical approach to the dynamic modelling of an underwater vehicle propeller in all four quadrants of operation, *Proceedings of the Institution of Mechanical Engineers, Part M: Journal of Engineering for the Maritime Environment*, *233*(1), 2019, 333-344.

[17] L. Paolucci, E. Grasso, F. Grasso, N. König, M. Pagliai, A. Ridolfi, A. Rindi, B. Allotta, Development and testing of an efficient and cost-effective underwater propulsion system, *Proceedings of the Institution of Mechanical Engineers, Part I: Journal of Systems and Control Engineering*, *233*(10), 2019, 1309-1328.

Biographies

Li Zhandong received the Ph.D. degree in aerospace engineering from Harbin Institute of Technology, China. He is currently a Research Scientist with the Department of Aerospace Sciences, Shenyang Aerospace University. His research interests include aircraft design and aerodynamic performance calculation.

Ma Shuang received the Ph.D. degree from the Harbin Institute of Technology in 2020. She is currently an Associate Professor and a Master's Supervisor with the School of Electronic and Information Engineering, Shenyang Aerospace University. Her research areas include electromagnetic field and microwave technology, field simulation analysis, and array signal processing.

Han Qi is currently pursuing the master's degree in transportation engineering with the College of Civil Aviation, Shenyang Aerospace University, China. Her research focuses on aerodynamic analysis and design of the flapping wing vehicle.

Li Jingkui received the Ph.D. degree from Northeastern University in 2006. He is an Associate Professor with the Civil Aviation College, Shenyang Aerospace University. His research interests is flight vehicle reliability.

Wang Chao received the B.S., M.S., and Ph.D. degrees from Harbin Institute of Technology in 2006, 2009, and 2016, respectively. He is an Associate Professor with the School of Mechanical Engineering, Dongguan University of Technology. His research interests are flight aerodynamics and flapping-wing micro aerial vehicles.